PROCEEDINGS OF THE ROYAL SOCIETY A

rspa.royalsocietypublishing.org

Research

Cite this article: Masuyama K, Barrett SRH. 2013 On the performance of electrohydrodynamic propulsion. Proc R Soc A 469: 20120623.
http://dx.doi.org/10.1098/rspa.2012.0623

Received: 22 October 2012
Accepted: 5 March 2013

Subject Areas:
fluid mechanics, power and energy systems

Keywords:
electrohydrodynamics, propulsion, ionized gases, electroaerodynamics

Author for correspondence:
Steven R. H. Barrett
e-mail: sbarrett@mit.edu

Electronic supplementary material is available at http://dx.doi.org/10.1098/rspa.2012.0623 or via http://rspa.royalsocietypublishing.org.

Royal Society Publishing
Informing the science of the future

On the performance of electrohydrodynamic propulsion

Kento Masuyama and Steven R. H. Barrett

Department of Aeronautics and Astronautics, Massachusetts Institute of Technology, 77 Massachusetts Avenue, Cambridge, MA 02139, USA

Partially ionized fluids can gain net momentum under an electric field, as charged particles undergo momentum-transfer collisions with neutral molecules in a phenomenon termed an ionic wind. Electrohydrodynamic (EHD) thrusters generate thrust by using two or more electrodes to ionize the ambient fluid and create an electric field. We characterize the performance of EHD thrusters of single- (SS) and dual-stage (DS) configurations. SS thrusters refer to a geometry using one emitter electrode, an air gap and a collector electrode with large radius of curvature relative to the emitter. DS thrusters add a collinear intermediate electrode. SS thruster performance was shown to be consistent with a one-dimensional theory. Increasing the gap length requires a higher voltage for thrust onset, generates less thrust per input voltage, generates more thrust per input current and most importantly generates more thrust per input power. A thrust-to-power ratio as high as approximately $100\,\mathrm{N\,kW^{-1}}$ was obtained. DS thrusters were shown to be more effective than their SS counterparts at producing current, leading to a smaller total voltage necessary for producing equal thrust. However, losses involving ion collection at the intermediate electrode led to reduced thrust-per-power compared with the SS thruster of equal length.

1. Introduction

Electrohydrodynamic (EHD) thrust in air, using a pair of asymmetrical electrodes under large potential differences of the order of tens of kilovolts, was first proposed by Brown [1]. The 'lifter' concept has recently been popularized, of which a typical configuration is shown in figure 1. The lifter has no moving parts;

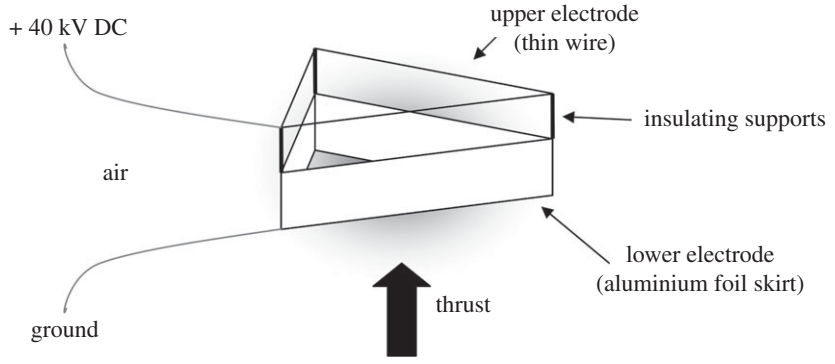

Figure 1. A typical 'lifter' design.

instead, the surrounding fluid is ionized and accelerated by a high potential gradient to generate an ionic wind. Direct emissions consist only of ionized products of the ambient fluid.

There exist few archival literature studies on the lifter, but a wealth of hobbyist information is available on the Internet as well as Army Research Laboratory [2] and National Aeronautics and Space Administration (NASA) [3] technical reports. In addition, other configurations have been tested [2–6], all operating with no moving parts or stored propellants. A related approach is the dielectric barrier discharge (DBD), which substitutes the interelectrode air gap with a thin dielectric layer [7]. DBD systems require a continuous solid surface and have been studied for flow control rather than for propulsion.

An ionic wind results from the net momentum gain in a mostly neutral fluid through momentum-transfer collisions with ions in an electric field. When a voltage in excess of the corona inception voltage (V_o) is applied across two electrodes with different radii of curvature ($r_e \ll r_c$), a non-uniform electric field with the largest magnitude in the vicinity of the smaller emitter electrode ignites a corona discharge that emits an ion stream. The ions are transported across the interelectrode gap at an average drift velocity $v_D = \mu E$, where μ is the ion mobility and E is the electric field magnitude, the result of a balance between the electrostatic force owing to the field and the drag force owing to the collisions. The ions are collected at the collector electrode and do not contribute to thrust, but the neutrals that gained energy in the collisions escape the system with net momentum along x, the direction from the emitter towards the collector.

Brown initially attributed the observed thrust force to a coupling between electromagnetism and gravity. Despite the faulty understanding of the physics, Brown had conceived of the 'lifter' design by the 1950s, consisting of a thin wire emitter separated from an aluminium foil collector with a lightweight non-conducting frame [8]. The concept of ionic wind was associated with EHD thrust as early as 1961, when Cheng's [9] one-dimensional model predicted a thrust that varied as the square of pressure. Christenson & Moller [4] developed an analytical model starting from the Navier–Stokes equations, whose predictions were confirmed by experiments using pointed pin emitters. The current density was seen to vary as $j \propto V(V - V_o)$, in agreement with the current output for corona discharges.

Recent studies have focused on improving the performance of EHD thrusters. Velocity and pressure distributions were simulated, using the method of characteristics in conjunction with boundary and finite-element methods [10,11]. Further modelling showed the dominance of electrostatic over hydrodynamic forces [12,13]. NASA studied EHD thrust under reduced pressure as well as in pure nitrogen or argon [3]. Thrust levels under positive and negative polarities as well as DC and AC currents were tested at the Sandia National Laboratories, Albuquerque, NM [14]. Different geometries for the emitter were tested, including a wire, pins with different spacing and razor blades [6]. Several studies have worked with more complex electrode geometries, including a wire–cylinder–plate configuration at École Centrale Paris, France [5], and a stacked multi-stage generator at Yonsei University, Seoul, Republic of Korea

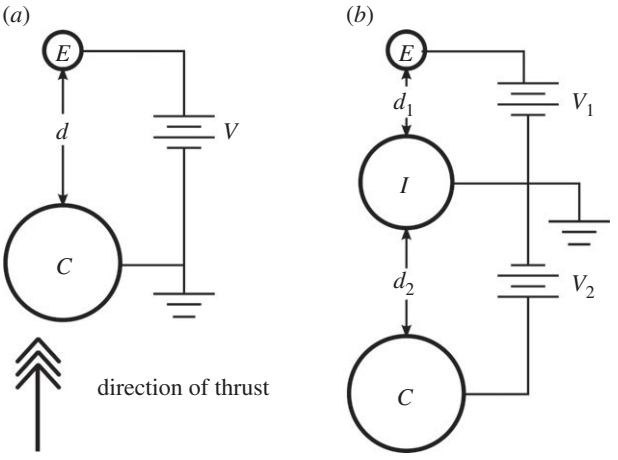

Figure 2. (*a*) Single-stage thruster electrodes. (*b*) Dual-stage thruster electrodes.

[15]. These tests demonstrated the feasibility of increasing thrust and flow velocity using more complex geometries.

The only previous experimental work on thrust generation (comparable to the 'lifter' concept) in the peer-reviewed literature is by Christenson & Moller [4] (although we note that their derivation for thrust assumes significant space charge and is not in agreement with ours). Until now, it had been concluded that EHD propulsion is too inefficient to be useful as a form of primary propulsion [4,15]. Here, we reopen this issue, noting that the appropriate metric for the 'efficiency' of stationary propulsors is thrust per unit power, F/P, and not propulsive efficiency (which is zero) or kinetic energy in the exhaust stream (which represents wasted energy). The ratio F/P is proportional to the inverse of thrust specific fuel consumption (SFC)—the conventional metric for comparing efficiency of propulsion systems in practice.

This paper characterizes the performance (especially F/P) of a single-stage (SS) 'lifter'-style thruster and a dual-stage (DS) design that involves a third intermediate voltage electrode collinear with the emitter and collector, as shown in figure 2. A one-dimensional theory with modifications to handle the DS case was developed, and experiments conducted with a 40 cm long linear thruster consisting of a 35 SWG wire emitter and an aluminium tube collector. We show that the F/P for a lifter is, both theoretically and experimentally, competitive with and likely to be higher than other propulsion technologies.

2. Theory

A one-dimensional model for an EHD thruster yields an expression for thrust in terms of the current throughput, assuming that the electrode length is long compared with the gap length d and electrode radii. Space charge effects, which we neglect, are low at corona ignition, but will become more pronounced as current and charge density increase. Defining current density using the ion drift velocity and a characteristic area A perpendicular to x, the total current is

$$I = \int j \cdot \mathrm{d}A = \int \rho \mu E \cdot \mathrm{d}A = \rho \mu E A, \tag{2.1}$$

where ρ is charge density, and other symbols are as previously defined. Taking the thrust to be equal to the Coulomb force on the volume of ions occupying the gap at any instant in time, for a SS thruster,

$$F_{\mathrm{SS}} = \int \rho E \, \mathrm{d}V = \int_0^d \rho E A \, \mathrm{d}x = \frac{Id}{\mu}. \tag{2.2}$$

Using the voltage–current relationship for corona discharges $I = CV(V - V_o)$ [16] with $C \propto \mu/d^2$ as defined by Cooperman [17], the thrust can be expressed as a function of voltage,

$$F_{SS} = \frac{C'V(V - V_o)}{d}, \tag{2.3}$$

where C' is an empirical value dependent on geometry.

The DS thruster introduces an intermediate potential electrode in between the emitter and collector. This allows for the decoupling of the two functions of the electric field: ionization and ion acceleration. The intermediate electrode is sized similar to the collector so as to maintain corona characteristics similar to the SS thruster, but no larger than the collector so as to not pose too large an area of interference. The first gap d_1 between the emitter and the intermediate electrode is raised to a large potential difference, so that a corona discharge ignites at the emitter. The second gap d_2 has a smaller field under which no further ionization occurs, but which will allow for the ions to travel across another potential drop and produce more thrust. In order to calculate thrust, the integration is carried out separately across each gap. Defining a factor $0 \leq \psi \leq 1$ to account for ion losses owing to collection at the intermediate electrode, the currents across the two gaps are related as $I_2 = \psi I_1$. Following the same arguments as mentioned earlier,

$$F_{DS} = \int_{d_1} \rho_1 E_1 A \, dx + \int_{d_2} \rho_2 E_2 A \, dx = \frac{I_1(d_1 + \psi d_2)}{\mu}. \tag{2.4}$$

(a) Thrust-to-power ratio, F/P

The thrust-to-power ratio was calculated as a metric to compare EHD thrust with competing technologies. This ratio is effectively the non-zero component of overall efficiency $\eta = Fv/P$, which equals zero for static tests with flight velocity $v = 0$, and is proportional to the inverse of thrust SFC.

The conventional aeronautical unit for SFC is pounds of fuel per hour per pound of thrust (lb lbf^{-1} h^{-1}), which is numerically equal to kg kgf^{-1} h^{-1}. Taking a fuel flow rate of $\dot{m}$ (kg s^{-1}), where the fuel has a lower calorific value (LCV) = 43 MJ kg^{-1},

$$\text{SFC (in lb lbf}^{-1}\text{h}^{-1}) = \frac{(P_{th}/\text{LCV}) \times 60^2}{F/g},$$

where $g = 9.81$ m s^{-2}, P_{th} is the heating rate assuming complete combustion and SI units are used except where otherwise specified. Thus, SFC can be related to F/P_{th} by

$$F/P_{th}(\text{in N kW}^{-1}) = \frac{0.821}{\text{SFC (in lb lbf}^{-1}\text{ h}^{-1})}. \tag{2.5}$$

From the January 2012 edition of the ICAO Engine Emissions Databank (http://easa.europa.eu/environment/edb/aircraft-engine-emissions.php), we calculated the mean SFC of all engines at 0.370 lb lbf^{-1} h^{-1}, the minimum at 0.253 lb lbf^{-1} h^{-1} and the maximum at 0.665 lb lbf^{-1} h^{-1} for rated thrust at take-off (sea-level static conditions). This implies that F/P_{th} is in the range 1.23–3.24 N kW^{-1} with a mean of 2.22 N kW^{-1}. Factoring out the engine's core thermal efficiency (typically approx. 50%) would approximately double these figures. Jet engines are designed for optimal performance at altitude rather than at take-off, but sea level was selected to match our experimental conditions. To take a specific example, the V2527-A5, which powers the A320 family of aircraft, produces 111.2 kN of thrust at take-off from each of its two engines, while burning 2×1.053 kg s^{-1} of fuel, or 45.3 MW per engine. This equates to 2.46 N kW^{-1}. Clearly, the scale of thrust production in this example is orders of magnitude higher than will be experimentally demonstrated in this paper, but, because large optimized jet engines are more efficient than bench-level experimental versions, this does help to provide context for F/P values for EHD.

The input power for a SS thruster is the product of the current and voltage outputs of the power supply. For the DS thruster, it is the sum of the same product for both power supplies, where the currents are related by ψ. As such,

$$\frac{F}{P_{\mathrm{SS}}} = \frac{Id}{\mu IV} = \frac{d}{\mu V} \tag{2.6}$$

and

$$\frac{F}{P_{\mathrm{DS}}} = \frac{I(d_1 + \psi d_2)}{\mu I_1(V_1 + \psi|V_2|)} = \frac{d_1 + \psi d_2}{\mu(V_1 + \psi|V_2|)}. \tag{2.7}$$

This implies that efficiency increases with air gap d, although the field strength needs to be sufficient to ignite the corona and low enough not to cause breakdown—or no thrust would be produced. It can also be seen that efficiency and thrust can be varied for a fixed air gap—for example, higher thrust by setting a higher voltage and a resulting lower efficiency at take-off versus lower voltage and thrust but higher efficiency under other conditions. We note that the effect of the bulk motion of air on current and power use has been neglected as we are considering static thrust in this paper.

In order to see the effect of ψ, equation (2.7) is expanded to first order,

$$\frac{d_1 + \psi d_2}{\mu(V_1 + \psi|V_2|)} = \frac{d_1 + d_2}{\mu(V_1 + |V_2|)} + \frac{(\psi - 1)(d_2 V_1 - d_1|V_2|)}{\mu(V_1 + |V_2|)^2} + O(\psi^2). \tag{2.8}$$

The first term on the right-hand side is independent of ψ and positive. The denominator of the second term is positive, but, with $0 \le \psi \le 1$ and $V_1/d_1 > V_2/d_2$ in order to ensure ionization only in the top gap, the numerator is negative. As such, a larger value of ψ corresponding to a larger portion of the current crossing the second gap is expected to minimize loss and generate a higher thrust-to-power value.

The quality of a specific thruster configuration can be quantified by a non-dimensional 'efficiency' comparing the experimental thrust-to-power ratio with the nominal theoretical prediction. In the case of a DS thruster, the ideal is that no ions are lost at the intermediate electrode, and thus ψ is set equal to unity. Then, for both SS and DS cases,

$$\Omega = \frac{F\mu V_{\mathrm{total}}}{P d_{\mathrm{total}}}, \tag{2.9}$$

where F and P are experimentally measured.

(b) Bilinear performance degradation

In previous experiments by Payton [18], an unexplained performance degradation was observed in a SS thruster (of the conventional 'lifter' design) at larger values of current. Equation (2.2) predicts a linear variation of thrust with current; however, above a threshold, the gradient $\mathrm{d}F/\mathrm{d}I$ was seen to decrease into a second linear regime. We hypothesize that, as the applied voltage is increased, a second corona discharge of opposite polarity is ignited at the collector. This is similar to transmission lines carrying opposite currents that have been known to ignite opposite polarity coronas [19]. The inception voltage V_{o2} is higher than the first (V_o) owing to the larger radius of curvature. The total current after the onset of the second corona is defined as the sum of the two opposite ion flows, $I = I^+ + |I^-|$, where the superscripts indicate the ion polarity and the emitter current is positive. Using a similar derivation as before, the thrust in this regime is

$$F_{\mathrm{BL}} = d\left(\frac{I^+}{\mu^+} - \frac{|I^-|}{\mu^-}\right). \tag{2.10}$$

This expression can be substituted into equation (2.6) to find the thrust-to-power expression for the degraded performance regime. The expression can be further simplified by defining a_1 and a_2 as the two gradients $\mathrm{d}F/\mathrm{d}I$. It is then possible to express $|I^-|$ in terms of the gradients, ion

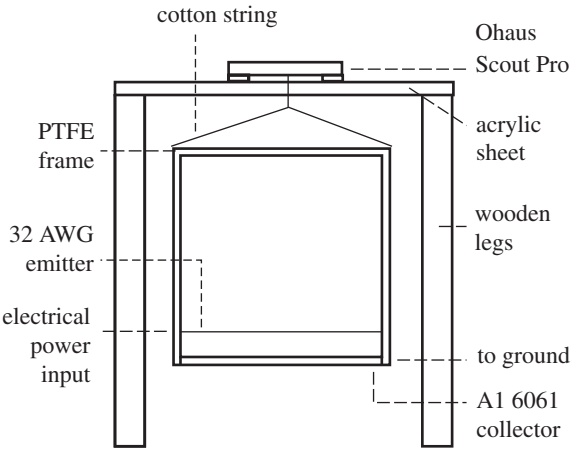

Figure 3. Overall experimental set-up.

mobilities and total current I, so that $|I^-| = I(1 - a_2/a_1)/(1 + \mu^+/\mu^-)$. Then, the thrust-to-power ratio in the degraded regime is

$$\frac{F}{P_{\mathrm{BL}}} = \frac{d}{V}\frac{I^+/\mu^+ - |I^-|/\mu^-}{I^+ + |I^-|} = \frac{d}{\mu^+ V}\frac{a_2}{a_1}, \quad V_{o2} < V. \tag{2.11}$$

Payton [18] found that net thrust continues to increase with applied voltage in this degraded regime (of lower $\mathrm{d}F/\mathrm{d}I$). This further implies the possible trade-off between high thrust and high efficiency for a fixed thruster geometry. This is in contrast to most jet engines, which are least efficient at low (e.g. idle) thrust.

3. Experimental set-up

In order to test both SS and DS thrusters, the experimental set-up shown in figure 3 was used. A square thruster frame with 40 cm sides, suspended from scales, was built of polytetrafluoroethylene (PTFE) and holes were placed at 1 cm increments (measured from the top point on the collector surface) to allow adjustment of the interelectrode gap. The collector making up one of the square sides was an aluminium 6061 tube with outer diameter of 6.35 mm. The emitter wire was a 32 AWG solid tinned copper wire. For the DS tests, the intermediate electrode was a 4 AWG copper wire. As the diameter of a 4 AWG wire at 5.189 mm is not negligible, the wires were arranged so that gap d_1 was adjustable at 1 cm increments from the top surface of the intermediate electrode, and the gap d_2 was also adjustable at 1 cm increments from the bottom surface of the intermediate electrode to the top surface of the collector. As all electrodes extended the length of the frame, each had a length $L = 40$ cm.

The thrust was measured, using an Ohaus Scout Pro digital scale with 600 g capacity and 0.01 g resolution. The thruster was hung from a hook on the underside of the scale, and the thrust was measured as a reduction in weight. The thruster weighed ≈ 240 g in the SS configuration and ≈ 320 g in the DS configuration.

Electrical power was supplied by a Matsusada AU120P2.5 for positive polarity and a Matsusada AU120N2.5 for negative polarity, both rated up to 120 kV and 2.5 mA. The power supplies had over-current protection for when arcing occurred. We used 3.5 digit displays to provide voltage and current readings.

4. Results

The presented data are averages from multiple trials. For plots with both SS and DS data, the open circles indicate SS and closed circles DS data.

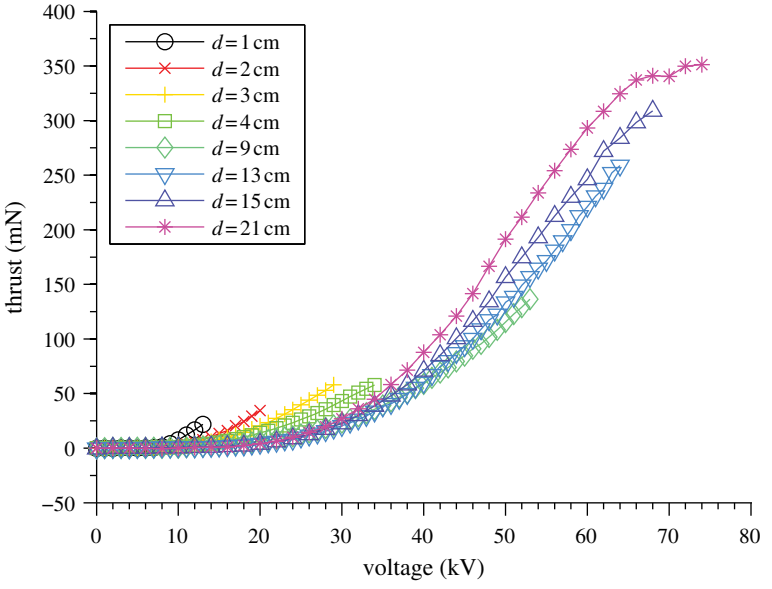

Figure 4. Voltage–thrust relationship for varying air gap, positive polarity. (Online version in colour.)

(a) Single-stage thrusters

Figure 4 shows the thrust for various gap lengths as positive voltage was varied. No thrust is seen at lower voltages, below the corona inception voltage for each geometry. The gap length term d in the denominator of equation (2.3) predicts a smaller thrust for a given voltage at larger gap lengths. The experimental data confirm this for gaps up to $d = 9$ cm, beyond which the trend reversed and higher thrust was seen for a given voltage at larger gap lengths. Smaller gap configurations are limited in their maximum output by the earlier onset of electrical breakdown and arcing, beyond which no thrust is produced. The trend reversal is not predicted by theory, and a possible explanation is the deviation of the thruster geometry from one dimension, or $L \gg d$.

Equation (2.3) also predicts a quadratic variation of the thrust with voltage. This is shown in figure 5 for a subset of gap lengths; larger gaps were omitted for clarity. Although the data do not significantly deviate from the overall linear fit, a systematic shift from overestimation to underestimation at higher voltages can be seen; we suggest that this is due to the aforementioned bilinear effect.

By using the current output data and ion mobility values as given by Tyndall & Grindley [20], the EHD thrust was compared with predictions by equation (2.2). The case shown in figure 6 is for the $d = 3$ cm case; as predicted, increasing d consistently generated higher thrust for a given current output. The two predictive lines correspond to the limiting cases of dry ($\mu_{\mathrm{dry}} = 2.155 \times 10^{-4}\,\mathrm{m^2\,V^{-1}}$) and saturated ($\mu_{\mathrm{sat}} = 1.598 \times 10^{-4}\,\mathrm{m^2\,V^{-1}}$) air. The data fit within the expected bounds for all gaps up to $d = 11$ cm, beyond which the data showed higher thrust than predicted; this effect may be related to the trend reversal seen in figure 4. Based on the accuracies of the voltage, current and thrust measurements, the relative errors for typical data points were 3.0 per cent, 12.5 per cent and 0.004 per cent, respectively. These uncertainties are all less than that of the inverse ion mobility, which has a variability of ±15% owing to humidity changes.

Figure 7 shows that larger gap lengths consistently perform at higher F/P, whereas, for each air gap size, F/P degrades with increasing thrust (and so increasing voltage) consistent with equation (2.6). For example, for $d = 21$ cm, F/P peaks at $110\,\mathrm{N\,kW^{-1}}$ (or averaging 68 $\mathrm{N\,kW^{-1}}$ for all power levels below 1 W), and reduces to $16\,\mathrm{N\,kW^{-1}}$ at 0.35 N of thrust, compared with values of approximately $2\,\mathrm{N\,kW^{-1}}$ for current aircraft engines (or approx. $4\,\mathrm{N\,kW^{-1}}$ if the core

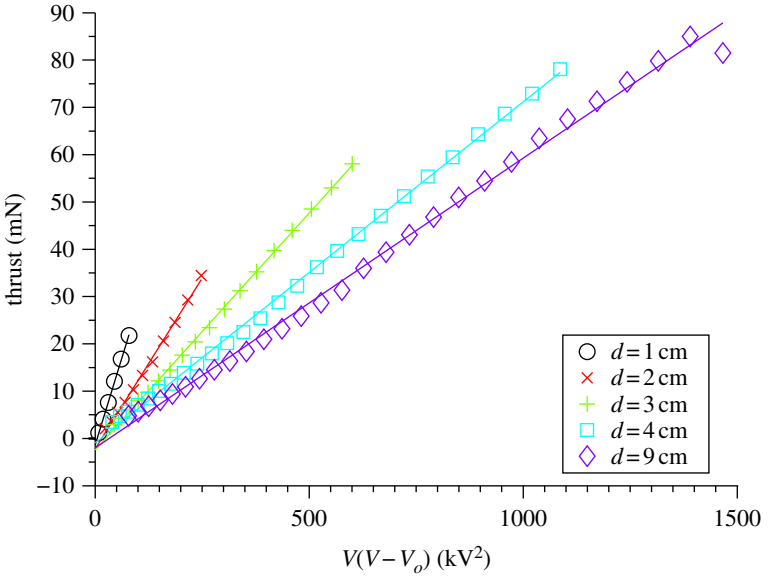

Figure 5. Linear relationship of thrust and $V(V - V_o)$ for single-stage thrusters. (Online version in colour.)

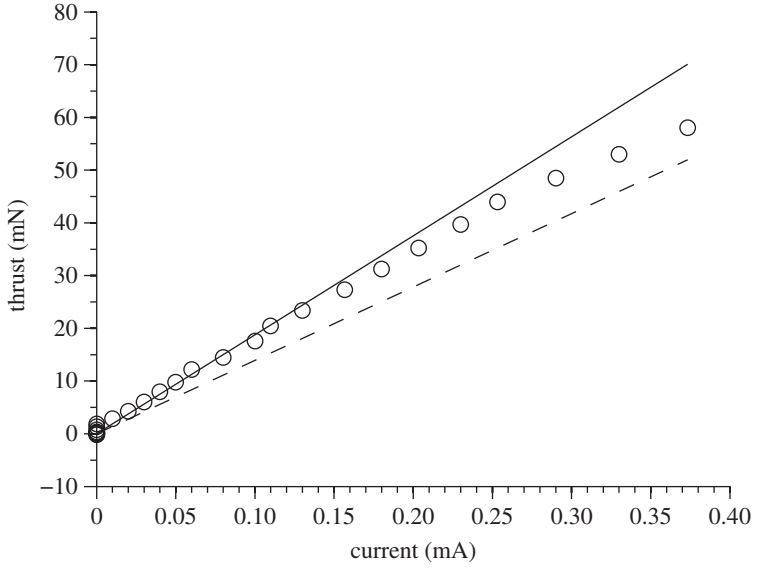

Figure 6. Comparison with theoretical prediction for $d = 3$ cm. Circles denote data; dashed line denotes dry air; solid line denotes saturated.

thermal efficiency is factored out). This does not imply that EHD thrusters are practical, but it does point to their potential for relatively high efficiency where efficiency is defined as thrust per unit power.

From a design perspective, characterization of the current, voltage and power required to generate a desired thrust as a function of a geometric variable is necessary. Figure 8 shows the results for a thrust of $F = 10$ mN. The inverse relationship of current and gap length assuming constant thrust and ion mobility in equation (2.2) is confirmed. The peak in voltage at a gap length of $d = 13$ cm corresponds to the reversal in trends in figure 4; the previously mentioned peak of 9 cm is true for higher thrust values. The variation of power also shows an inverse relationship with gap length. The power reading of 0 at $d = 21$ cm is the result of the current output being less

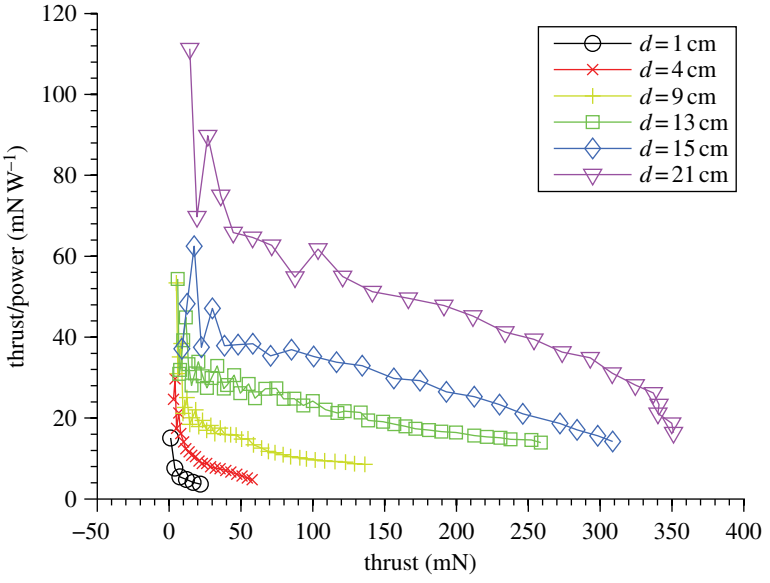

Figure 7. Variation in thrust/power as a function of thrust. For an alternative version of this figure that contains additional experimental results, see the electronic supplementary material. (Online version in colour.)

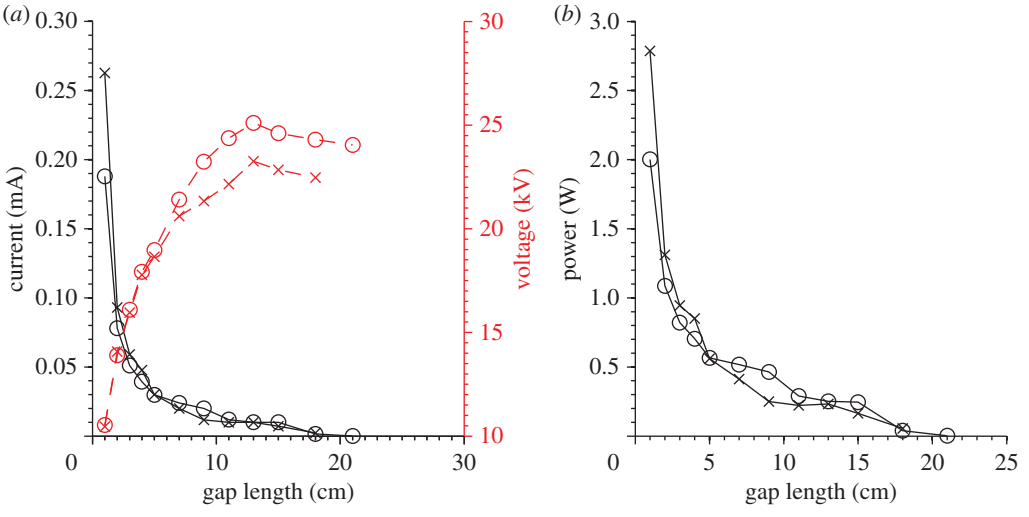

Figure 8. Required current (*a*), voltage (*a*) and power (*b*) for $F = 10$ mN with positive (circles) and negative polarities (multiplication symbols). (Online version in colour.)

than the 0.01 mA resolution of the ammeter. Larger gap lengths are able to generate a given thrust for less power, but there is diminishing return as d is increased to higher values.

Figure 8 also shows the similar performance of positive and negative polarity excitation. The trends shown in earlier figures also held true under negative voltage. For all gap lengths other than $d = 1$ cm, the difference in required current was less than 0.02 mA. The voltages were almost identical up to $d = 7$ cm, and between 2 and 2.5 kV less for the negative polarity at larger gaps. The negative corona output a higher current for a given voltage, with standard deviations ranging from 0.007 to 0.016 mA for gaps up to 5 cm. The thrust per volt was higher for the negative case, with an average difference of 1.403 mN over the voltage domain for the $d = 5$ cm case. However, owing to the higher output current, the power requirement for a given thrust is similar in both polarities, as shown in figure 8*b*.

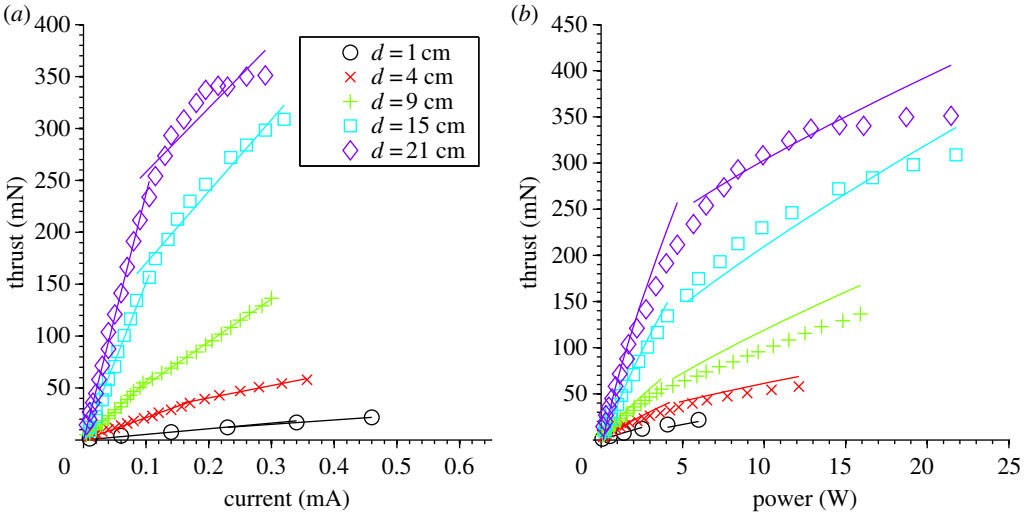

Figure 9. (*a*) Bilinear fit for thrust–current relationship. (*b*) Bilinear prediction for thrust–power relationship. For an alternative version of this figure that contains additional experimental results, see the electronic supplementary material. (Online version in colour.)

(b) Bilinear theory results

The thrust variation with current is bilinear, with an initial linear variation of gradient a_1 and, beyond some threshold, a second linear regime with reduced gradient a_2. The threshold was selected as a point on the thrust versus current plot and perturbed so that the residuals for the two linear fits were minimized. Figure 9*a* shows the two linear fits for each geometry. The gradients correspond to the amount of additional thrust generated for a unit increase in the current output. All linear fits for both regimes, except in the case of $d \geq 15$ cm, have coefficients of determination $R^2 > 0.98$. The gap values greater than 15 cm show a nonlinear decay in performance, causing the bilinear model to have a less accurate fit than at smaller gaps.

The data are compared with the thrust-per-power predictions in figure 9*b*. The predictions, shown by lines, were calculated from a_1 and a_2 and integrated over power. The gap in the two segments of predictions is an artefact of the use of empirical values for power. The bilinear model predicts a piecewise decrease in performance beyond the onset of the reverse current, greater than the decrease attributable to the voltage term in the denominator of equation (2.6). The measured data demonstrate this sharp degradation, and, in most cases, the actual losses are greater than predicted. The initial regime is fitted more accurately by the model, and the location of the sharp degradation is in agreement. The causes of the further losses in the second regime are unknown and require further study.

(c) Dual-stage thrusters

DS thrusters can be compared with SS thrusters for two sets of requirements: electrical or volumetric. In order to maintain similar electrical properties, the cases of $d = d_1$ can be studied. Figure 10 shows the variation of total field $E = V_{\text{tot}}/d_{\text{tot}}$ and thrust-to-power as the second gap d_2 is increased for a thrust of 5 mN and $d_1 = 1$ cm. The corona inception voltage is not offset significantly from the SS case of $d = 1$ cm owing to the locally high field in between the emitter and intermediate electrodes. DS tests were conducted at three values of V_2, and all cases required a lower overall voltage than the SS case, shown by the open circle at 9.2 kV cm^{-1} in figure 10*a*. For the cases of $V_2 = 5$ or 10 kV, the thrust-to-power ratio monotonically decreased with d_2, with all tested values of d_2 except 13 cm showing higher thrust per power than the SS case. With $V_2 = 20$ kV, the trend shifts upward. The thrust-to-power ratio is less than the SS case for $d_2 = 3$ or

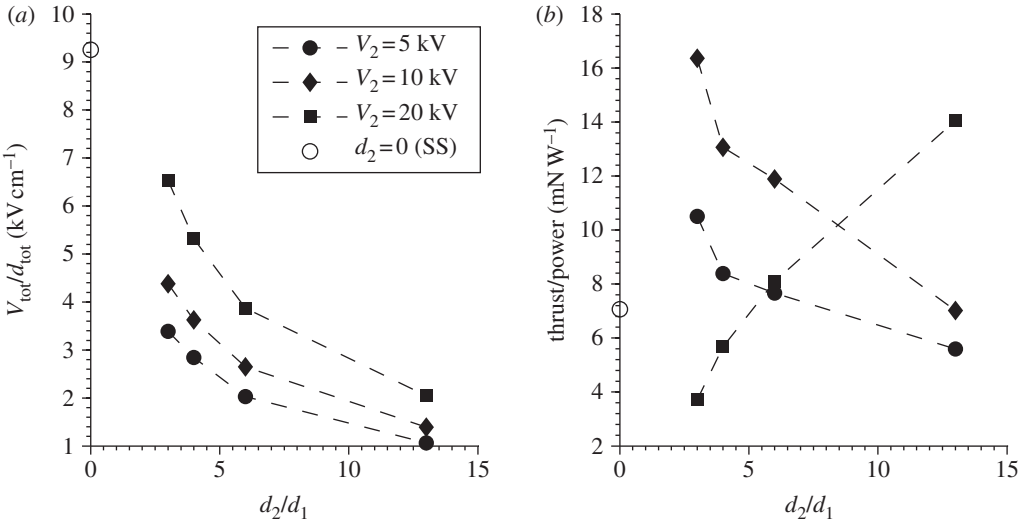

Figure 10. (*a*, *b*) Variation of V/d and F/P with d_2/d_1 for $F = 5$ mN, $d_1 = 1$ cm.

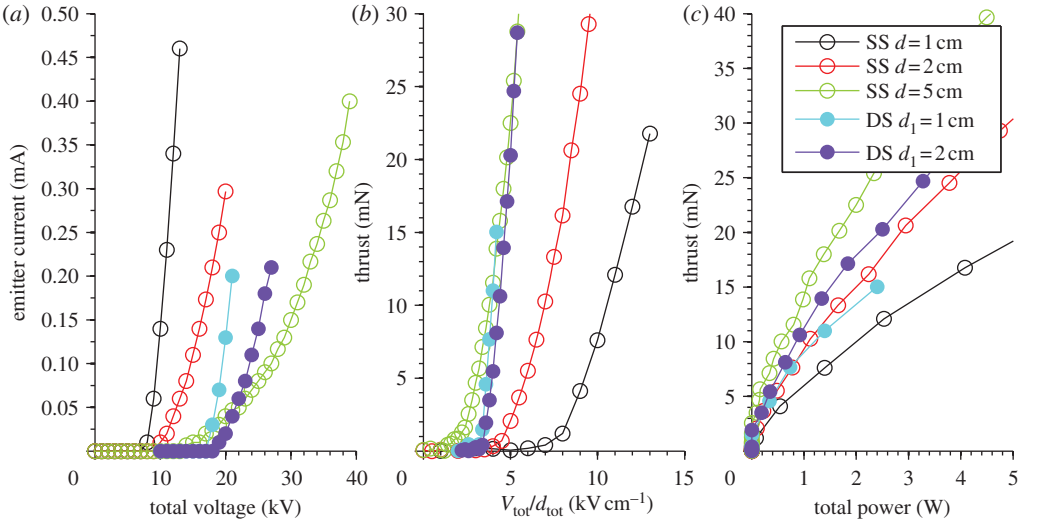

Figure 11. (*a–c*) Current and thrust variation with d_1 for $d_{tot} = 5$ cm, $V_2 = 10$ kV. (Online version in colour.)

4 cm, but increases to double the SS value at the maximum tested gap of $d_2 = 13$ cm. This reversal in trend is the result of changes in current distribution, characterized by ψ.

The total gap length can be created by different combinations of d_1 and d_2. Figure 11 compares two cases with $d_{tot} = 5$ cm along with SS cases of $d = 1, 2$ and 5 cm (the two values of d_1 and d_{tot}). For the DS cases, data are shown for $V_2 = 10$ kV.

Smaller d_1 shows a higher current for a given total voltage owing to the higher field strength in the ionizing first gap. Comparing the gradients of the two DS cases with the SS cases corresponding with $d = d_1$ shows that the first gap controls the voltage–current properties of the corona discharge, although there is a voltage offset owing to the additional field created in the second gap. The effectiveness of the average field in creating thrust for the cases of $V_2 = 10$ kV matches the SS case of equal total gap length. From the thrust versus power plot, it is seen that the

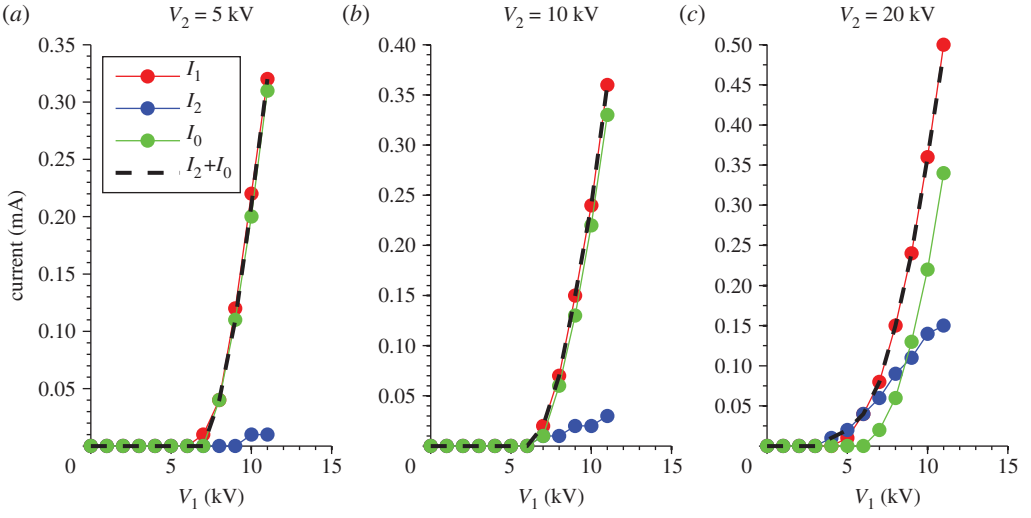

Figure 12. (*a–c*) Current distribution for $d_1 = 1$ cm, $d_2 = 3$ cm, bare electrode. (Online version in colour.)

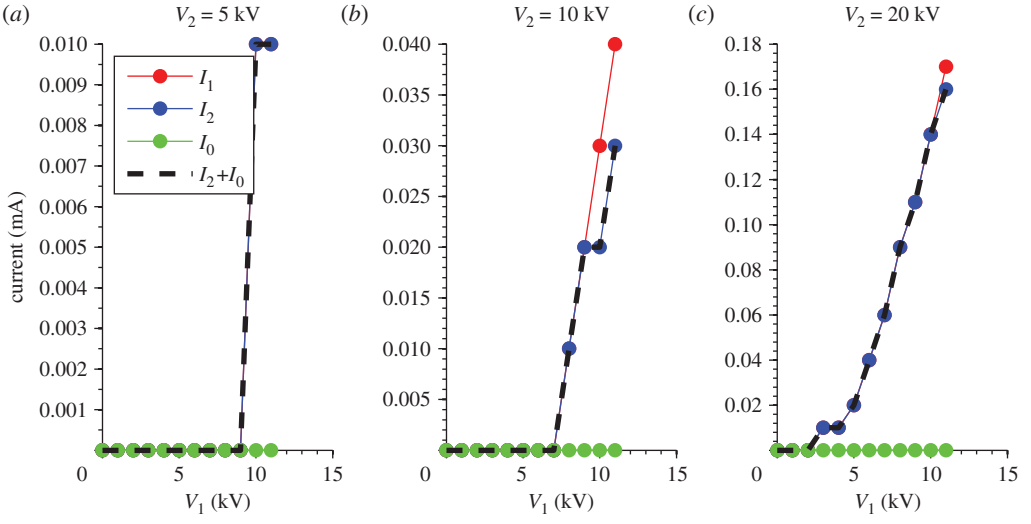

Figure 13. (*a–c*) Current distribution for $d_1 = 1$ cm, $d_2 = 3$ cm, insulated electrode. (Online version in colour.)

DS configuration improves the thrust-to-power ratio over the $d = d_1$ case, but that losses prevent the ratio from reaching the ratio obtained with the $d = d_1 + d_2$ case.

For specificity, we compare the SS thruster with $d = 5$ cm against the DS thruster with $d_1 = 2$ cm and the same overall size. It can be seen that (i) the DS thruster F/P is approximately 20 per cent lower than the SS thruster of the same overall size, but still higher than the smaller SS thrusters, and (ii) that the DS thruster tracks the SS thruster in terms of thrust (F) versus average field strength ($V_{\mathrm{tot}}/d_{\mathrm{tot}}$). In this specific case, if only the ionization stage were used (SS with $d = 2$ cm) F/P would be approximately 10 per cent lower and would require nearly double the applied total voltage for a given thrust.

An ammeter was connected in series with the intermediate electrode (I_0), and the currents through the emitter (I_1) and collector (I_2) were used to calculate ψ. Figure 12 shows the measured current distribution for $d_1 = 1$ cm and $d_2 = 3$ cm using the bare copper intermediate electrode. The fraction ψ varies with both V_1 and V_2. For $V_2 = 5$ kV, ψ is zero for $V_1 \leq 10$ kV, and never exceeds 0.01. Setting $V_2 = 20$ kV is the only case in which ψ becomes significant, ranging from 1 just above

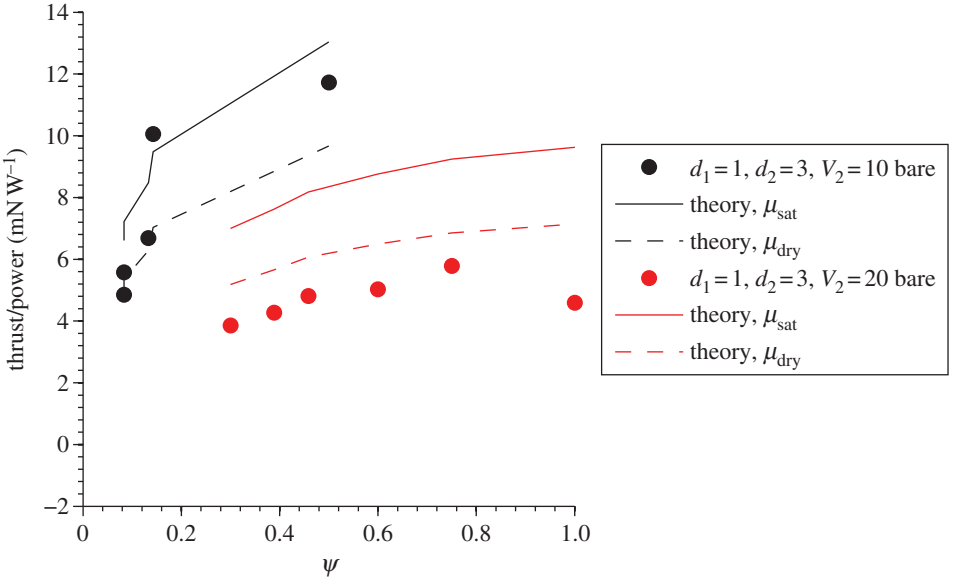

Figure 14. Thrust-to-power variation with ψ for $d_1 = 1$ cm, $d_2 = 3$ cm. (Online version in colour.)

corona inception to 0.3 just before arcing; this is then the only tested configuration making use of both gaps, explaining the trend reversal in figure 10.

Higher values of ψ are obtained by reducing ion collection at the intermediate electrode. Using an insulated 10 AWG wire with similar radius to the bare copper wire, the current distributions shown in figure 13 were obtained. Current fraction ψ is equal to 1 for most values of V_1 and V_2. However, the absolute value of the emitted current was reduced, from 0.5 mA with the bare electrode to 0.17 mA, thus reducing thrust. Using the experimental values of V_1, V_2 and ψ, the thrust-to-power ratio was calculated according to equation (2.7). As seen in figure 14, the ratio increases with ψ both in theory and in experiment. The sharp corners in the theoretical predictions are artefacts of the use of the experimental values of ψ.

Figure 15 shows the variation in Ω with thrust for a subset of the SS thrusters. The general trend is an improvement with increased gap length. These results show that over aspect ratios of 40 : 1 to 2 : 1, $\Omega \sim 1$. It is also apparent that for the near two-dimensional cases $\Omega \approx 1$, whereas when the aspect ratio is about 2 : 1 the value increases to $\Omega \approx 2$. In general, Ω decreases towards unity as thrust increases (limited by breakdown). Taken together, these results suggest that $\Omega = 1$ is a first approximation for performance at the limit of thrust, whereas at lower thrust conditions $\Omega > 1$, implying an efficiency higher than the one-dimensional theory predicts.

Figure 16 shows Ω for DS thrusters for $V_2 = 5$, 10 or 20 kV with various geometric configurations. For $V_2 = 5$ or 10 kV, all configurations show decreasing Ω as thrust increases. Furthermore, as d_2 increases, Ω is reduced (consistent with reducing ψ). Changes in d_1 and d_2 affect Ω differently, as the $d_1 = 2$ cm consistently shows higher Ω than the 1 cm design with the same d_2. The dependence on d_1 is amplified by a smaller d_2, with an average difference in Ω of ≈ 0.3 for $d_2 = 3$ cm, as opposed to ≈ 0.15 for $d_2 = 13$ cm with $V_2 = 5$ kV. The case $V_2 = 10$ kV shows a larger spread with configuration than the $V_2 = 5$ kV cases. The configuration of lowest Ω with both voltages, $d_1 = 1$ cm and $d_2 = 13$ cm, shows a similar asymptote near 0.1. However, the configuration of highest Ω of $d_1 = 2$ cm and $d_2 = 3$ cm shows $\Omega \approx 0.75$ at $F = 25$ mN for $V_2 = 10$ kV as opposed to ≈ 0.6 at the same thrust level for $V_2 = 5$ kV. For $V_2 = 20$ kV, some of the trends change. In the cases of $d_2 = 3$ or 4 cm, Ω increases with thrust to an asymptote in the range 0.5–0.6. The longer gaps show Ω decreasing with thrust, with the $d_2 = 6$ cm case tending towards asymptotes around 0.4 and the $d_2 = 13$ cm case dropping below 0.3. In all cases, the maximum thrust achieved before breakdown was approximately the same as a SS thruster of length d_1.

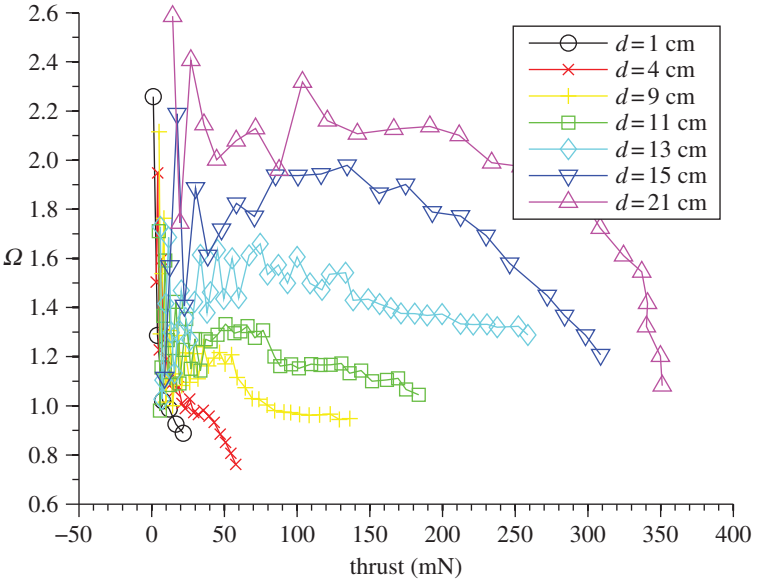

Figure 15. Variation of Ω with thrust, single stage. (Online version in colour.)

These results imply that to first order the F/P achievable scales with length d_{tot} of the thruster for both SS and DS thrusters, where d_{tot} has varied by a factor of 20 in experiments in this work. However, if a DS configuration is used, then the increased F/P relative to a SS configuration is reduced by a factor Ω_{DS}. Specifically, if a fixed supply voltage is available, F/P is increased by a factor

$$\frac{(F/P)_{\mathrm{DS}}}{(F/P)_{\mathrm{SS}}} = \frac{d_{\mathrm{tot}}}{d_{\mathrm{SS}}}\frac{\Omega_{\mathrm{DS}}}{\Omega_{\mathrm{SS}}} = \left(1 + \frac{d_2}{d_1}\right)\frac{\Omega_{\mathrm{DS}}}{\Omega_{\mathrm{SS}}}$$

when comparing a DS thruster of length d_{tot} with a SS thruster of size d_1. This suggests an alternative potential configuration for EHD thrusters, variable geometry—for example, extension of a secondary collector when high efficiency is required. Additionally, decoupling of ionization and acceleration stages may have practical advantages—for example, allowing for alternative ionization schemes, or, given a limited supply voltage, allowing for a larger gap length (and thus efficiency) than otherwise may be possible while sustaining sufficient field strength to ignite the corona in the first stage.

5. Concluding remarks

The 'lifter' concept has recently been popularized, but it has not been subjected to extensive study. We experimentally validated a one-dimensional theory of lifter performance, with particular consideration of thrust-to-power ratio, F/P. Both the conventional SS lifter is considered as well as a DS design in which the ionization and acceleration stages are partly decoupled.

The ratio F/P for EHD propulsion was experimentally shown to reach $110\,\mathrm{N\,kW^{-1}}$. Modern jet engines produce approximately $2\,\mathrm{N\,kW^{-1}}$ by comparison, although helicopters are higher. Conceptually, the reason for this high efficiency (in the F/P sense) of EHD is because the same thrust can be produced with a narrow high-speed jet (as with jet engines), which leaves kinetic (and thermal) energy in the exhaust stream, or a low-speed wind over a large area.

Many trends predicted by the one-dimensional theory were confirmed for both SS and DS designs. In particular (i) thrust varies as the square of voltage above the corona inception; (ii) thrust varies bilinearly with current, with degraded performance upon secondary corona inception; (iii) thrust-to-power ratio increases with gap length and decreases with thrust; and (iv) DS designs allow for higher efficiency for a given maximum supply voltage.

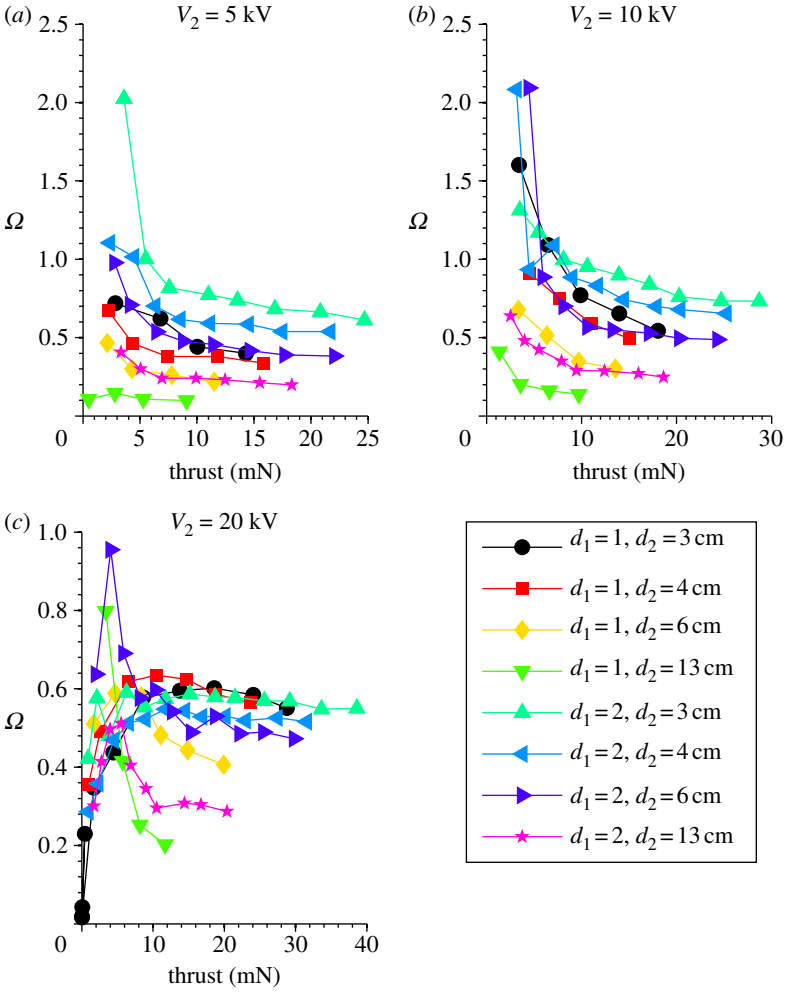

Figure 16. (*a–c*) Variation of Ω with thrust, dual stage. (Online version in colour.)

Finally, we ask what will happen in non-static tests. If we take an example, where $\mu = 2 \times 10^4\ \mathrm{m^2\,V^{-1}}$ and $E = 350\ \mathrm{kV\,m^{-1}}$, then

$$\frac{F}{P} = \frac{1}{\mu E} = 14.3\ \mathrm{N\,kW^{-1}},$$

which is just below the values experimentally determined. The overall efficiency $\eta = Fv/P$, where v is flight velocity, is zero here. Now factoring flight velocity into current so that $I = \rho A(\mu E + v)$, and taking an illustrative value of $v = 70\ \mathrm{m\,s^{-1}}$ (comparable to an aircraft at take-off and equal to μE in this example), we find that

$$\frac{F}{P} = \frac{1}{\mu E + v} = 7.13\ \mathrm{N\,kW^{-1}}.$$

In this case, overall efficiency is $\eta = Fv/P = 50\%$, compared with the V2527-A5's value of 17 per cent at the same forward speed (although if only power delivered by the core were being compared, the overall efficiency of the two propulsion systems would be similar). This yields an interesting observation for EHD propulsion (provided that the 'jet' velocity is $v + \mu E$, as has been implicitly assumed)—that $\eta \to 1$ as v increases, reaching 2/3 at $v = 140\ \mathrm{m\,s^{-1}}$ in this example. We note that an ion mobility suitable for near-sea-level pressure has been applied here. Assuming that

ion mobility increases in inverse proportion to pressure and taking a representative flight speed of 250 m s^{-1} at 10 km altitude under International Standard Atmosphere conditions, $\eta = 48\%$, which is comparable to modern jet engines at cruise. (If E were halved, then $\eta = 65\%$.)

While we have demonstrated—experimentally and in part by theoretical extrapolation—that EHD propulsion may provide practical levels of efficiency, what has not been addressed in this paper is whether EHD propulsion can produce the thrust density necessary to be useful. This is unknown and will be the subject of future work.

References

1. Brown TT. 1928 *A method of and an apparatus or machine for producing force or motion*. UK Patent no. GB300311 (A).
2. Bahder TB, Fazi C. 2003 Force on an asymmetric capacitor. Technical Report ARL-TR-XXX, Army Research Laboratory, Adelphi, MD.
3. Canning FX, Melcher C, Winet E. 2004 Asymmetrical capacitors for propulsion. Technical Report NASA/CR-2004-213312, National Aeronautics and Space Administration, Washington, DC.
4. Christenson EA, Moller PS. 1967 Ion-neutral propulsion in atmospheric media. *AIAA J.* **5**, 1768–1773. (doi:10.2514/3.4302)
5. Colas DF, Ferret A, Pai DZ, Lacoste DA, Laux CO. 2010 Ionic wind generation by a wire–cylinder–plate corona discharge in air at atmospheric pressure. *J. Appl. Phys.* **108**, 103306. (doi:10.1063/1.3514131)
6. Wilson J, Perkins HD, Thompson WK. 2009 An investigation of ionic wind propulsion. Technical Report NASA/TM-2009-215822, National Aeronautics and Space Administration, Washington, DC.
7. Braun EM, Lu FK, Wilson DR. 2008 A critical review of electric and electromagnetic flow control research applied to aerodynamics. In *Proc. 39th Plasmadynamics and Laser Conference, Seattle, WA, 23–26 June 2008*. Red Hook, NY: Curran Associates, Inc.
8. Brown TT. 1960 *Electrokinetic apparatus*. US Patent no. US2949550.
9. Cheng SI. 1961 The glow discharge as an advanced propulsion device. Technical Report AeroChem TP-33, Office of Naval Research, Arlington, VA.
10. Zhao L, Adamiak K. 2005 Numerical analysis of forces in an electrostatic levitation unit. *J. Electrostat.* **63**, 729–734. (doi:10.1016/j.elstat.2005.03.036)
11. Zhao L, Adamiak K. 2006 EHD gas flow in electrostatic levitation unit. *J. Electrostat.* **64**, 639–645. (doi:10.1016/j.elstat.2005.10.017)
12. Martins AA, Pinheiro MJ. 2011 Modeling of an EHD corona flow in nitrogen gas using an asymmetric capacitor for propulsion. *J. Electrostat.* **69**, 133–138. (doi:10.1016/j.elstat.2011.02.002)
13. Martins AA, Pinheiro MJ. 2011 On the influence that the ground electrode diameter has in the propulsion efficiency of an asymmetric capacitor in nitrogen gas. *Phys. Plasmas* **18**, 033512. (doi:10.1063/1.3562874)
14. Miller WM, Miller PB, Drummond TJ. 2009 Force characterization of asymmetrical capacitor thrusters in air. In *Frontiers of propulsion science: progress in astronautics and aeronautics*, vol. 227 (eds MG Millis, EW Davis), pp. 293–327. New York, NY: American Institute of Aeronautics and Astronautics.
15. Kim C, Park D, Noh KC, Hwang J. 2010 Velocity and energy conversion efficiency characteristics of ionic wind generator in a multistage configuration. *J. Electrost.* **68**, 36–41. (doi:10.1016/j.elstat.2009.09.001)
16. Fridman A, Kennedy LA. 2004 *Plasma physics and engineering*. New York, NY: Taylor & Francis.
17. Cooperman P. 1960 A theory for space-charge limited currents with application to electrical precipitation. *AIEE Trans.* **79**, 47–50.
18. Payton J. 2010 Electrohydrodynamic propulsion. Fourth-year undergraduate project, Engineering Department, University of Cambridge, UK.
19. Fridman A, Gutsol A, Cho YI. 2007 Non-thermal atmospheric pressure plasma. In *Transport phenomena in plasma* (eds A Fridman, YI Cho), pp. 1–134. Advances in Heat Transfer, vol. 40. Amsterdam, The Netherlands: Elsevier.
20. Tyndall AM, Grindley GC. 1926 The mobility of ions in air. *Proc. R. Soc. Lond. A* **110**, 341–364. (doi:10.1098/rspa.1926.0019)